

Molecular dynamics simulation of reversibly self-assembling shells in solution using trapezoidal particles

D. C. Rapaport*

Department of Physics, Bar-Ilan University, Ramat-Gan 52900, Israel

(Dated: November 19, 2012)

The self-assembly of polyhedral shells, each constructed from 60 trapezoidal particles, is simulated using molecular dynamics. The spatial organization of the component particles in this shell is similar to the capsomer proteins forming the capsid of a T=1 virus. Growth occurs in the presence of an atomistic solvent and, under suitable conditions, achieves a high yield of complete shells. The simulations provide details of the structure and lifetime of the particle clusters that appear as intermediate states along the growth pathway, and the nature of the transitions between them. In certain respects the growth of size-60 shells from trapezoidal particles resembles the growth of icosahedral shells from triangular particles studied previously, with reversible bonding playing a major role in avoiding incorrect assembly, although the details differ due to particle shape and bond organization. The strong preference for maximal bonding exhibited by the triangular particle clusters is also apparent for trapezoidal particles, but this is now confined to early growth, and is less pronounced as shells approach completion along a variety of pathways.

PACS numbers: 87.16.Ka, 81.16.Fg, 02.70.Ns

I. INTRODUCTION

Self-assembly at the molecular scale occurs in an environment where thermal noise provides strong competition to the forces that drive growth; in this respect such microscopic processes differ significantly from their macroscopic counterparts. While direct experimental observation of the details of supramolecular self-assembly is not readily achieved, computer simulation, assuming the availability of simplified models capable of capturing the essential details, ought to be able to supply information that is otherwise inaccessible.

The formation of the capsid shells enclosing the genetic material of spherical viruses [1, 2] is a well-known example of self-assembly. The organization of capsid structures is simplified and the construction specifications are minimal because the shells are assembled from multiple copies of one or a small number of different capsomer proteins [3] and the structures satisfy icosahedral symmetry. This information, however, provides little help in trying to determine the assembly steps involved in forming the capsid. Even a highly simplified version of the problem, in which capsomers spontaneously and reversibly form complete shells under *in vitro* conditions free of genetic material [4–7], remains opaque. The robustness of self-assembly [8] makes understanding the process in simplified environments a worthwhile endeavor, especially since analogous processes, inspired by the mechanisms employed by the virus itself, could provide a basis for nanoscale chemical packaging with possible therapeutic uses involving targeted delivery.

Molecular dynamics (MD) simulation [9], with its ability to capture both the spatial and time-dependent prop-

erties of interacting many-body systems, is capable of providing access to the shell assembly pathways themselves and predicting the varying populations of partially complete structures; this provides, in principle, a direct link with experiment [10]. A simplified capsomer particle for use with MD can be represented by a set of soft spheres rigidly arranged to produce an effective molecular shape consistent with packing into a closed shell, together with a set of interaction sites where attractive forces between particles act. Reduced descriptions of this kind are designed to mimic the relevant features of real capsomers that consist of folded proteins – large molecules whose exposed surfaces have relatively complex landscapes that are able to fit together to form the closed, strongly bound capsids.

The initial MD studies of this problem [11, 12] were severely restricted by limited computational resources and consequently focused on demonstrating the feasibility of assembly in the absence of solvent, subject to the restriction that the process was irreversible (meaning that bonds, once formed, are unbreakable). Shells of size 60 were grown from triangular and trapezoidal particles, the latter corresponding to the structure of T=1 viruses, as well as shells of size 180 resembling T=3 viruses. This was followed by a more computationally demanding MD study of reversible assembly (in which bonds break when sufficiently stretched) for T=1 shells [12], but while reversibility is more reasonable from a physical perspective the approach required that smaller particle clusters be decomposed at regular intervals to avoid kinetic traps due to a lack of unbonded particles.

Increased computer performance permitted the inclusion of an explicit atomistic solvent [13–15] thereby eliminating the need for enforced decomposition, but only for the case of triangular particles assembling into 20-particle icosahedral shells. The explicit solvent provides a means for collision-induced breakup of clusters without needing

*Electronic address: rapaport@mail.biu.ac.il

them to come into direct contact; it also adds a diffusive component to the otherwise ballistic particle motion, and serves as a heat bath for absorbing and redistributing energy released when particles bond. These simulations demonstrated that self-assembly proceeds via a sequence of reversible stages, with a high yield of complete shells and a strong preference for minimum-energy intermediate clusters. Though seemingly paradoxical, reversibility provides the key to efficient self-assembly due to its ability to prevent subassemblies becoming trapped in configurations inconsistent with continued correct growth.

The goal of the present work is to extend the previous MD study of icosahedral shell assembly in solution to the larger $T=1$ shells. Increased shell size offers a broader range of growth possibilities, permitting ‘entropic’ effects to compete more strongly with the energetic preferences dominating the growth of smaller shells. Comparing the outcomes of growth simulations involving different shell sizes can provide insight into how this factor influences growth and, in particular, which aspects of growth observed previously are common to both the smaller and larger shells.

An alternative, even more simplified representation of capsomers can be based on spherical particles, using directional interactions, and an implicit solvent represented by stochastic forces [16]. The motivation for the present study, based on extended rather than spherical particles, is that the capsomers are themselves extended bodies, with complex shapes generally tailored to conform to the shells. Use of extended particles means that the interaction range need not exceed the particle size, allowing the design to be tuned to ensure that bonding forces are maximized only when particles are correctly positioned and oriented, while avoiding bond formation in other situations; this is reflected by the absence of any incorrect growth in the simulations described here. Another difference is in the solvent representation; the question of whether the explicit solvent used here could be replaced by stochastic forces has not been examined, although the former has the advantage that motions of particles not in direct contact are correlated through the solvent, as would be the case in a real fluid. In the case of block copolymers it has been shown that self-assembly simulations based on implicit and explicit solvents lead to very different outcomes [17]; different solvent dynamics may also help explain the fact that enhanced pentamer stability is observed, as expected, when assembling triangular particles using an explicit solvent [13], but not when the solvent is implicit [18].

MD simulations using complete all-atom descriptions of the capsomer proteins [19] are another possibility, but because of their complexity they are presently limited to very short time intervals, adequate only for examining preassembled shells. A further simplified MD approach involves quasi-rigid bodies formed from hard spheres [20]. Monte Carlo simulations have been used in assembly studies of particles of various shapes [21–23]. A number of theoretical techniques for studying capsid structure

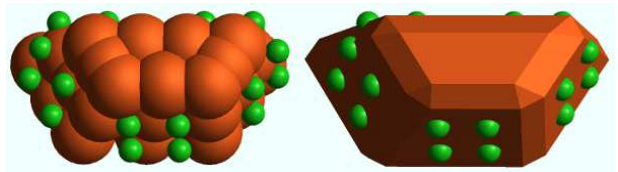


FIG. 1: (Color online) The component spheres and effective shape of the trapezoidal particle; the small spheres denote the attraction sites.

have been explored, including thin shells [24], tiling [25], particles on spheres [26], stochastic kinetics [27], elastic networks [28], and nucleation theory [29], as has a combinatorial approach to the pathways [30]. Focusing on the kinetic aspects of subassembly concentration is another approach [31, 32] that is also used in interpreting experimental results [33, 34] and analyzing the effects of reversibility on growth [35].

II. METHODS

The two components in the MD system are the self-assembling model capsomer particles and the solvent atoms. The particle, shown in Fig. 1, features an extended, highly specific shape, together with multiple attraction sites. It is formed from a rigid array of soft spheres arranged to have the effective shape of a trapezoidal truncated pyramid, and 60 copies can be packed to make a closed shell; the design was introduced in the earlier solvent-free study [12]. The lateral faces contain the attractive interaction sites involved in bond formation and determine the dihedral angles of the assembled shell; two of the adjacent short lateral faces are perpendicular to the plane of the particle, allowing three adjacent particles to form a planar triangular face, whereas the other two faces are inclined to provide the required dihedral angle between adjacent triangular shell faces.

Two kinds of interactions are used in the model [15]. Soft-sphere repulsion is provided by the truncated Lennard-Jones potential,

$$u_s(r) = \begin{cases} 4\epsilon[(\sigma/r)^{12} - (\sigma/r)^6 + 1/4] & r < r_c = 2^{1/6}\sigma \\ 0 & r \geq r_c \end{cases} \quad (1)$$

where r is the separation, $r_c = 2^{1/6}\sigma$ is the interaction cutoff, with σ approximating the effective sphere diameter, and ϵ determines the energy scale. Solvent atoms are represented using the same interaction. In standard reduced MD units, $\sigma = 1$ and $\epsilon = 1$, while both the solvent atoms and particle spheres have unit mass. The length of the irregularly shaped particle (distance between the centroids of the bonding sites in the opposite short faces) is 3.6 (MD units), the width (between bonding sites in opposite long and short faces) 2.1, and the depth (extent of top and bottom spheres) 2.7. In Fig. 1 the component

spheres are drawn with unit diameter.

The attractive interaction responsible for assembly consists of two parts that blend together smoothly, a short-range, finite-depth harmonic well and a medium range, inverse-power attraction,

$$u_a(r) = \begin{cases} e(1/r_a^2 + r^2/r_h^4 - 2/r_h^2) & r < r_h \\ e(1/r_a^2 - 1/r^2) & r_h \leq r < r_a \end{cases} \quad (2)$$

Attraction acts selectively and occurs only between those sites in face pairs that would be adjacent in a correctly assembled shell and, of these, only between correspondingly positioned sites. Site pairs in the bound state tend to lie near the bottom of the well ($r = 0$), but there is nothing to prevent escape if sufficiently excited. The attraction changes form at the crossover distance $r_h = 0.3$, and ceases entirely at the cutoff $r_a = 3$. Individual pair interactions have no directional dependence, but when acting together they contribute to correct particle positioning and orientation. The only parameter varied in $u_a(r)$ is the overall attraction strength e .

Standard MD methods [9] are used for the simulations. The force calculations employ neighbor lists for efficiency, with separate lists used for the soft-sphere repulsive forces and the longer-range attractions. Once all the forces acting on the soft spheres and attraction sites of the particles have been evaluated they are combined to produce the total forces and torques required for the translational and rotational equations of motion; these are solved using leapfrog integration, with a time step of 0.005 (MD units). Constant-temperature MD is used to prevent heating due to exothermic bond formation. The boundaries of the simulation region are periodic and the region size is determined by the overall number density. Preparation of the initial state and other details appear in [13].

Methods for cluster analysis were described previously [14]. For any two particles, if each of their four corresponding attraction-site pairs are closer than r_b then the particles are considered bonded; setting $r_b=0.5$ leads to quantitative results consistent with direct observation, namely no spurious bond breakage or inappropriate bonds. The bond count of a cluster, used in the analysis below, is the total number of bonded particle pairs.

III. RESULTS

A. Shell production

The present simulations consider systems in which the total number of trapezoidal particles and solvent atoms is 125 000, contained in a cubic region with an overall number density of 0.1; the particle concentration is 2.2% (by number – corresponding to a volume fraction of 0.045), enough, in principle, for 45 complete shells. The runs cover a series of interaction strength values, e , resulting in a variety of outcomes. Thermostatting maintains a

TABLE I: Final cluster distributions for different interaction strengths, e , expressed as mass fractions and grouped by cluster size into monomers, clusters in different size ranges, and complete shells; the fractions with the majority populations are shown in bold and the run lengths are included.

e	Time steps	Cluster mass fraction					
		Size: 1	2–10	11–30	31–50	51–59	60
0.080	72×10^6	0.997	0.003	0.	0.	0.	0.
0.085	256×10^6	0.628	0.001	0.	0.	0.	0.371
0.090	251×10^6	0.175	0.	0.	0.017	0.022	0.786
0.095	146×10^6	0.019	0.	0.039	0.256	0.642	0.044
0.100	149×10^6	0.008	0.002	0.085	0.473	0.432	0.

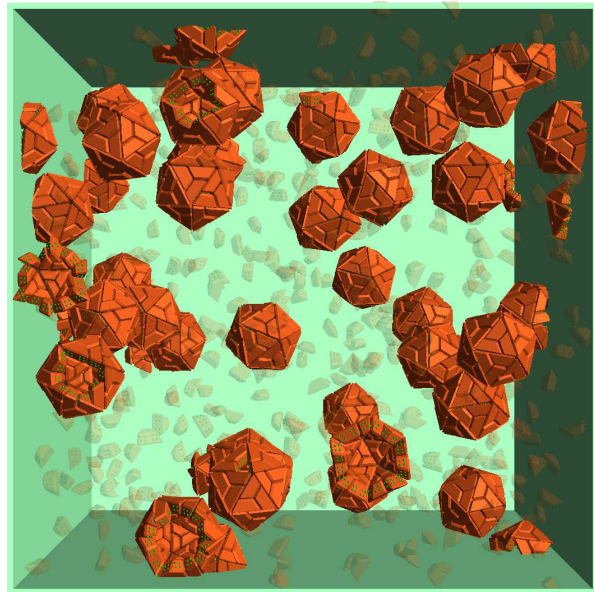


FIG. 2: (Color online) Late state of the $e=0.090$ run, with the solvent omitted and particles not in complete shells shown semitransparently; complete shells that cross periodic boundaries appear open, an artifact of the visualization.

constant temperature of 0.667, equivalent to unit average translational kinetic energy per particle or solvent atom; the corresponding total energy drops as bonding occurs, e.g., for $e=0.090$ it falls from 1 to 0.7 over the course of the run.

The final cluster distributions and run lengths are summarized in Table I. For increasing e , over a relatively narrow range, these vary from essentially no growth, through various yields of complete shells, to cases in which there is abundant growth but no full shells. The values for $e=0.090$ correspond to 36 complete shells, amounting to an 80% yield. In this run, and for $e=0.085$ where there is also significant shell production, the almost complete absence of intermediate size structures when growth ends is especially notable. The highest shell yield for trapezoidal particles is achieved at e approximately $0.6 \times$ the corresponding triangular value [13], so that the overall

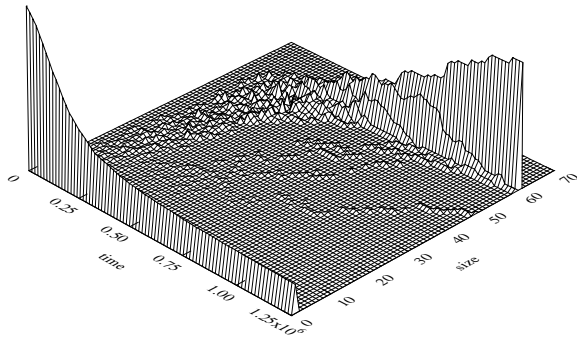


FIG. 3: Time-dependent cluster size distribution (mass fraction) for $e=0.090$; the final peaks correspond to monomers and complete shells; each grid interval along the time axis (MD units) corresponds to $\sim 3 \times 10^6$ time steps.

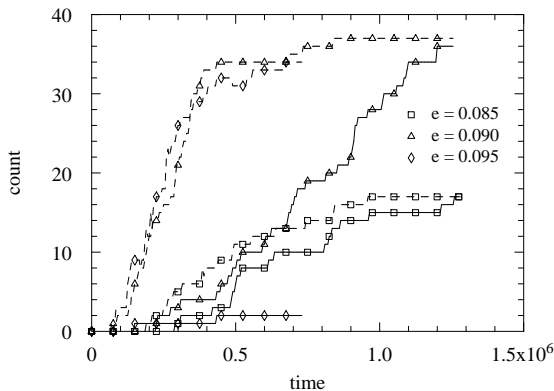


FIG. 4: Number of complete shells (solid lines) and combined number of complete shells and large (size > 50) clusters (dashed lines) as functions of time.

binding energies per particle in the two cases are similar.

Fig. 2 shows the $e=0.090$ system once shell growth is practically complete. The fact that there is ample space for shell growth without crowding is apparent. The mean separation of bound attraction sites is only 0.024 (MD units). Complete shells are likely to enclose solvent atoms since there are no interactions that prevent this.

B. Cluster size distributions

The time-dependent cluster size distributions exhibit the same e -dependence noted for triangular particles [13]. Fig. 3 shows the results for $e=0.090$; although appearing similar to the icosahedral results, the time and size scales are considerably larger. Two prominent features are the sharp bimodality of the distribution and the absence of significant populations of intermediate size clus-

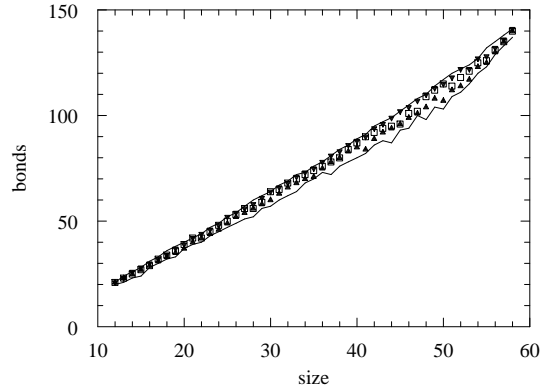


FIG. 5: Bond counts for different cluster sizes ($e=0.090$); solid lines show the minimum and maximum observed counts, triangles the ranges of counts accounting for $> 80\%$ of cases, and squares the most frequent counts.

ters. Since clusters commence growing at different times there is no evidence for coordinated growth [31].

Cluster growth rates are sensitive to e ; the time-dependence of the number of complete shells and the combined number of complete shells and large clusters with size > 50 are shown in Fig. 4. For $e=0.085$ and 0.090, the convergence of the cluster numbers towards the end of the runs, irrespective of the different yields, reflects the fact that almost all large clusters grow to completion. Entirely different behavior occurs for $e=0.095$, where there are many large but incomplete clusters.

C. Bond distributions

A simple way of classifying intermediate structures is based on the bond counts defined earlier. Fig. 5 shows the measured variation in bond count for each cluster size over the range of sizes where this is significant ($e=0.090$). The results include the minimum and maximum bond counts, the ranges of counts accounting for over 80% of cases – these generally either include the maximum counts or lie just 1 or 2 below them – and the most frequent counts. Bond count depends only weakly on e ; the average count (over all cluster sizes) for, e.g., $e=0.1$ is smaller by approximately 0.9 (1%), reflecting fewer breakup events that could increase the fraction of more highly bonded clusters.

In the case of smaller clusters, the results are similar to icosahedra [13], namely a strong preference for maximum bond counts, with over 90% of the clusters below size 12 in this category. This effect is less pronounced for larger clusters. Furthermore, unlike icosahedral shells, structures formed by trapezoidal particles during the later stages of assembly are sufficiently large to allow multiple,

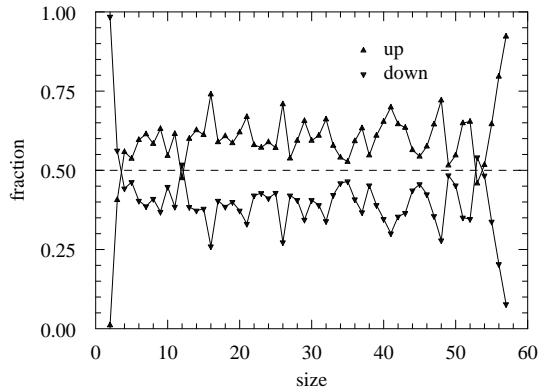


FIG. 6: Event fractions corresponding to cluster size changes ($e=0.090$).

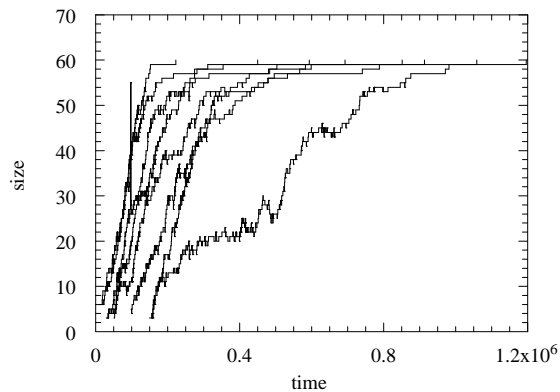


FIG. 7: Growth histories of several shells; the large spike for one of the shells corresponds to a temporary merger of two big clusters.

well-separated zones where growth occurs independently (see Fig. 10 below).

D. Reversible bonding

Growth proceeds by means of a sequence of size-change events. Fig. 6 shows the fraction of events experienced by clusters of each size that correspond to up (growth) and down (breakup) size changes. Practically all size changes are of unit magnitude (details not shown). With the notable exception of dimers, and to a lesser extent trimers, growth is almost always more likely than breakup. Reversibility is important, but, unlike the triangular particles [13, 15] where the preferred size-change direction varies strongly with cluster size, for trapezoidal parti-

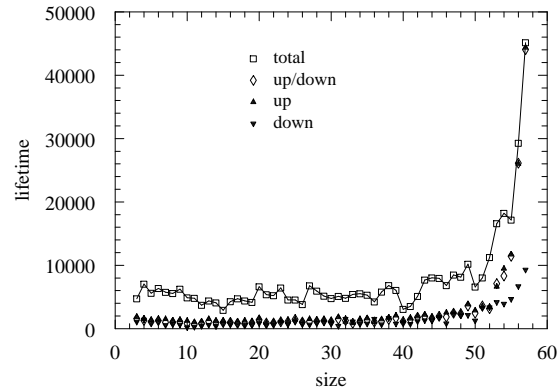


FIG. 8: Total and intermittent cluster lifetimes (MD units), the latter also subdivided according to whether, in the subsequent event, the size change is up or down ($e=0.090$).

cles the preference for specific intermediate cluster sizes is reduced. The effect of reversibility on assembly is apparent in the growth histories shown in Fig. 7, where size fluctuations are prominent.

Table II shows the e -dependence of P_g , the probability of the next event being growth, and T_i , the average intermittent lifetime (the elapsed time between consecutive size-changing events) for the smallest clusters. The extremely low dimer P_g ($\sim 1\%$) implies that practically all dimer events amount to disappearance. Trimers are more stable than dimers, as reflected in the reduced breakup probability ($= 1 - P_g$) and a T_i value over $20\times$ larger; in contrast, for triangular particles [13] the earliest appearance of enhanced stability occurs for pentamers. The mean P_g values for larger sizes are included; for the 5–20 size range P_g increases with e as before, but for 21–50 the trend is unclear because falling monomer availability also affects the behavior.

Fig. 8 shows several kinds of cluster lifetime measurements, namely the intermittent lifetime T_i , which is also subdivided according to whether the subsequent event is a size increase or decrease, and the total time a cluster exists at a given size T_t (the sum over T_i). The value of T_i is based on all clusters appearing during the run, while T_t is obtained by tracking those clusters that correspond to the complete shells and other large subassemblies present at the end. (For the final two assembly stages, $T_t = 8.8 \times 10^4$ and 1.7×10^5 .) Comparison with triangular particles [14] shows reduced variability in T_t at intermediate sizes. The ratio of T_t to T_i is an estimate of the number of occasions a reversibly growing cluster reaches a particular size; for most sizes this typically happens several (3–6) times.

TABLE II: Average growth probabilities, P_g , and intermittent lifetimes (MD units), T_i , of the smallest clusters, for different e ; mean P_g values for larger clusters are also shown.

Size	e	P_g	T_i
2	0.080	0.006	39
	0.085	0.007	49
	0.090	0.014	62
	0.095	0.015	79
3	0.080	0.193	790
	0.085	0.284	1106
	0.090	0.446	1684
	0.095	0.516	1951
4	0.080	0.261	1093
	0.085	0.412	1580
	0.090	0.554	1813
	0.095	0.712	2223
5–20	0.085	0.538	
	0.090	0.599	
	0.095	0.642	
21–50	0.085	0.601	
	0.090	0.609	
	0.095	0.586	

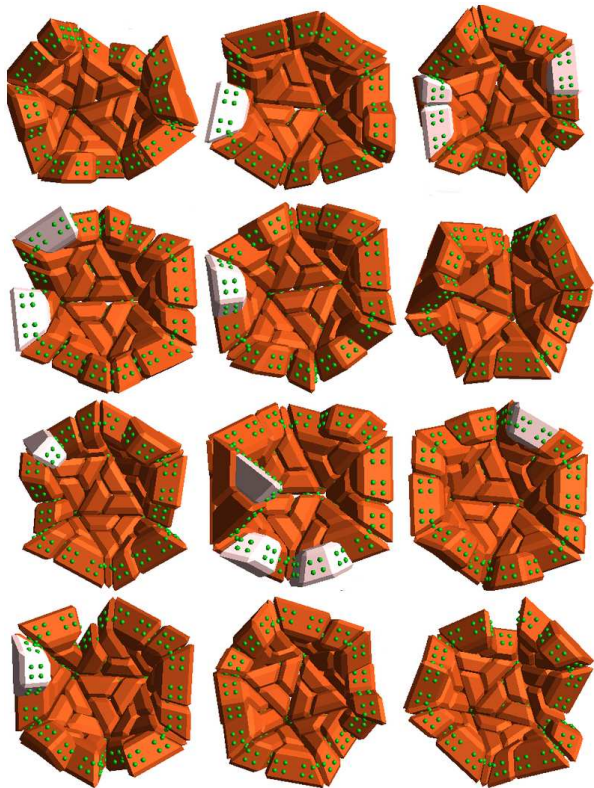


FIG. 9: (Color online) Clusters of size 30, oriented to show their perimeters; the majority of the particles are also present in the final shells into which the clusters develop, with the few that escape shown in a lighter color/shade.

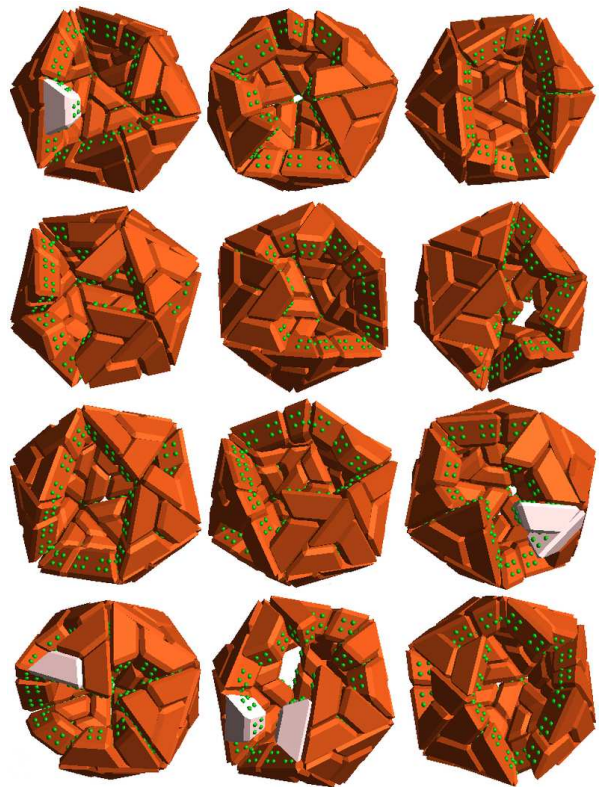


FIG. 10: (Color online) Clusters of size 50, oriented to show the variation in hole number and shape.

E. Visualizing structure and growth

Examination of the intermediate clusters reveals considerable variation in morphology not evident from the bond counts alone. A montage of 30-particle clusters, each recorded the moment it first reached this size, is shown in Fig. 9. The perimeters have a variety of profiles with different degrees of roughness, and the number of bonds observed in clusters of this size ranges from 57 to 64 (80% have 60–64 bonds). None of the clusters have holes, although deep boundary indentations are potential precursors. Fig. 10 shows a selection of incomplete shells containing 50 particles. The opportunity for independent growth in separate zones of the structure is increased relative to icosahedral shells, and bond counts vary between 103 and 117 (80% have 107–115 bonds). The results are for $e=0.090$, but the other e values are similar. These incomplete shells do not resemble the neatly truncated spheres employed in theoretical analysis [4, 29].

The image sequence in Fig. 11 shows several stages in the growth of one of the $e=0.090$ shells. Here, as the shell begins to close, the single large opening becomes several smaller holes that eventually fill. Although growth by merging of extended clusters is a rare event, it is occasionally observed; Fig. 12 shows an example in which clusters of size 32 and 15 join. Not all such mergers per-

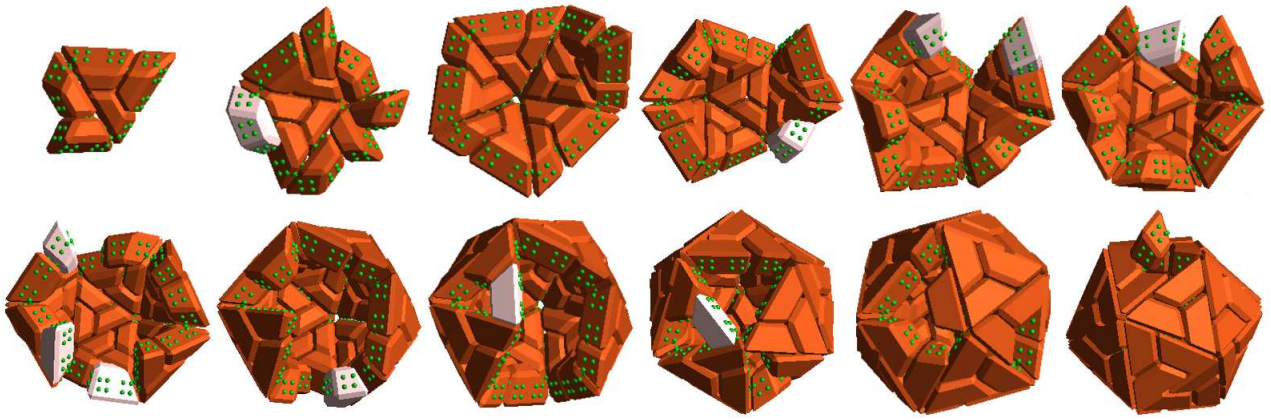


FIG. 11: (Color online) An example of shell growth (color coding as in Fig. 9); in the final image the shell is about to close.

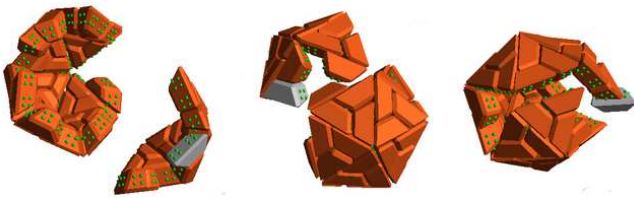


FIG. 12: (Color online) Stages in the successful merging of two clusters; the last image shows the state an instant before final bonding.

sist, however, and the spike in Fig. 7 corresponds to a shortlived merger.

IV. CONCLUSION

The 60-particle shells that self-assemble from trapezoidal particles considered in the present work share some

of the previously observed growth characteristics of icosahedral shells. All steps in the assembly process, except at the very end, show strong reversibility, a characteristic of systems only weakly out of equilibrium. Reversible bonding has a major influence on shell production, by ensuring an adequate monomer supply and allowing error correction to avoid incorrect structures. There is a clear preference for the most highly bonded clusters during early growth, but while this effect persists throughout the growth of icosahedral shells, it is less prominent here. In both cases growth is rate-limited by dimer formation; however, the different particle shapes lead to changes in the intermediate cluster properties. The larger shells considered here offer more opportunity for independent growth in well-separated zones of the partial structures. Although the present focus is on the self-assembly dynamics of polyhedral shells, key aspects of the observed behavior ought to be relevant for other kinds of microscopic assembly phenomena.

-
- [1] F. H. C. Crick and J. D. Watson, *Nature (Lond.)* **177**, 473 (1956).
- [2] D. L. D. Caspar and A. Klug, *Cold Spring Harbor Symp. Quant. Biol.* **27**, 1 (1962).
- [3] T. S. Baker, N. H. Olson, and S. D. Fuller, *Microbiol. Mol. Biol. Rev.* **63**, 862 (1999).
- [4] C. Berthet-Colominas, M. Cuillel, M. H. J. Koch, P. Vachette, and B. Jacrot, *Eur. Biophys. J* **15**, 159 (1987).
- [5] P. E. Prevelige, D. Thomas, and J. King, *Biophys. J.* **64**, 824 (1993).
- [6] G. L. Casini, D. Graham, D. Heine, R. L. Garcea, and D. T. Wu, *Virology* **325**, 320 (2004).
- [7] A. Zlotnick and S. Mukhopadhyay, *Trends in Microbiol.* **19**, 14 (2011).
- [8] D. L. D. Caspar, *Biophys. J.* **32**, 103 (1980).
- [9] D. C. Rapaport, *The Art of Molecular Dynamics Simulation* (Cambridge University Press, Cambridge, 2004), 2nd ed.
- [10] D. Endres and A. Zlotnick, *Biophys. J.* **83**, 1217 (2002).
- [11] D. C. Rapaport, J. E. Johnson, and J. Skolnick, *Comp. Phys. Comm.* **121**, 231 (1999).
- [12] D. C. Rapaport, *Phys. Rev. E* **70**, 051905 (2004).
- [13] D. C. Rapaport, *Phys. Rev. Lett.* **101**, 186101 (2008).
- [14] D. C. Rapaport, *J. Phys.: Condens. Matter* **22**, 104115 (2010).
- [15] D. C. Rapaport, *Phys. Biol.* **7**, 045001 (2010).
- [16] M. F. Hagan and D. Chandler, *Biophys. J.* **91**, 42 (2006).
- [17] J. R. Spaeth, I. G. Kevrekidis, and A. Z. Panagiotopoulos, *J. Chem. Phys.* **134**, 164902 (2011).
- [18] J. P. Mahalik and M. Muthukumar, *J. Chem. Phys.* **136**, 135101 (2012).
- [19] P. L. Freddolino, A. S. Arhipov, S. B. Larson,

- A. McPherson, and K. Schulten, *Structure* **14**, 437 (2006).
- [20] H. D. Nguyen, V. S. Reddy, and C. L. Brooks III, *Nano Letters* **7**, 338 (2007).
- [21] T. Chen, Z. Zhang, and S. C. Glotzer, *Proc. Natl. Acad. Sci. USA* **104**, 717 (2007).
- [22] A. W. Wilber, J. P. K. D. A. A. Louis, E. G. Noya, M. A. Miller, and P. Wong, *J. Chem. Phys.* **127**, 085106 (2007).
- [23] I. G. Johnston, A. A. Louis, and J. P. K. Doye, *J. Phys.: Condens. Matter* **22**, 104101 (2010).
- [24] J. Lidmar, L. Mirny, and D. R. Nelson, *Phys. Rev. E* **68**, 051910 (2003).
- [25] R. Twarock, *J. Theor. Biol.* **226**, 477 (2004).
- [26] R. Zandi, D. Reguera, R. F. Bruinsma, W. M. Gelbart, and J. Rudnick, *Proc. Natl. Acad. Sci. USA* **101**, 15556 (2004).
- [27] M. Hemberg, S. N. Yaliraki, and M. Barahona, *Biophys. J.* **90**, 3029 (2006).
- [28] S. D. Hicks and C. L. Henley, *Phys. Rev. E* **74**, 031912 (2006).
- [29] R. Zandi, P. van der Schoot, D. Reguera, W. Kegel, and H. Reiss, *Biophys. J.* **90**, 1939 (2006).
- [30] P. Moisant, H. Neeman, and A. Zlotnick, *Biophys. J.* **99**, 1350 (2010).
- [31] A. Y. Morozov, R. F. Bruinsma, and J. Rudnick, *J. Chem. Phys.* **131**, 155101 (2009).
- [32] M. F. Hagan and O. Elrad, *Biophys. J.* **98**, 1065 (2010).
- [33] A. Zlotnick, J. M. Johnson, P. W. Wingfield, S. J. Stahl, and D. Endres, *Biochemistry* **38**, 14644 (1999).
- [34] P. van der Schoot and R. Zandi, *Phys. Biol.* **4**, 296 (2007).
- [35] A. Zlotnick, *J. Mol. Biol.* **366**, 14 (2007).